STATIC ANALYSIS OF FGM CYLINDRICAL SHELLS UNDER LOCAL LOAD USING QUASI-3D HIGHER-ORDER SHEAR DEFORMATION THEORY

Tran Van Hung*, Tran Ngoc Doan, Vu Quoc Tru, Nguyen Anh Tuan, Vu Xuan Duc

Le Quy Don Technical University

Abstract

The paper presents static analysis results of functionally graded material (FGM) cylindrical shells under concentrated load by an analytical approach. The basic equations are formulated based on a higher-order shear strain theory, taking into account the effects of transverse shear strain and stress. The one-dimensional material distribution in the thickness direction follows Voigt's power law. In this article influences of several geometric parameters and material distribution coefficients on the stress state of FGM cylindrical shells are considered. Based on the analysis results at the clamped boundary zone, the local load concentration is found, and the transverse normal stress is demonstrated to be considerable at this zone.

Keywords: *Cylindrical shells; FGM; higher-order shear/normal deformation theory; stress-strain state; stress concentration phenomenon.*

1. Introduction

Functionally Graded Materials (FGMs) are advanced composites, in which there are two or more phases and have mechanical properties that vary smoothly in the direction of distribution [1]. Typically, FGMs consist of two phases that are metal and ceramic. One of the outstanding advantages of FGMs is the smooth change in the material composition, which can eliminate stress interruption and thus prevents material delamination [2]. Moreover, FGMs possess great advantages over conventional composite materials when working at high temperature conditions, as well as in high humidity environments. Due to these above-mentioned pros, FGMs are applied in many fields of science and engineering such as aerospace, nuclear power, and dental medicine, etc. [3].

Analyses of FGM structures are of great interest and have drawn attention of many scientists. Computational models for FGM plates and shells may be developed based on the classical plate theory (CPT) or Kirchhoff theory [4], the first-order shear deformation theory (FSDT) introduced by Mindlin [5], the third-order shear deformation theory

* Email: hungsr79@gmail.com

(TSDT) by Reddy [6], with many authors interested as Nguyen [7, 8], higher-order shear deformation theories and the three-dimensional elastic theory, etc. The use of CPT and FSDT in calculations requires the addition of shear correction factors, and sometimes cannot produce accurate results at complex load locations. TSDT also ignores horizontal deformation and stress in the calculation model. To enhance the fidelity of the computational model, it is necessary to employ the quasi-3D higher-order shear strain theory, which takes into account the effects of normal shear deformation and stress, especially in areas with complex loads. At present, the use of the quasi-3D high shear strain theory is still rarely used, especially for shell structures.

In this paper, the authors use the quasi-3D higher-order shear deformation theory to investigate the stress-deformation state of FGM cylindrical shells. The displacement field is expressed by a third-order polynomial of the plane displacement and a quadratic polynomial of the displacement in the thickness direction. The analytical method is used to solve this problem, and Voigt's power function is employed to model the material distribution in the thickness direction [9].

2. Theoretical basics

Consider an FGM cylindrical shell with a thickness of $2h$, and other geometric parameters are shown in Fig. 1. Assume that the shell is subjected to radial local loads $q^{\pm}(\xi,\theta)$, and $\xi = x / R$.

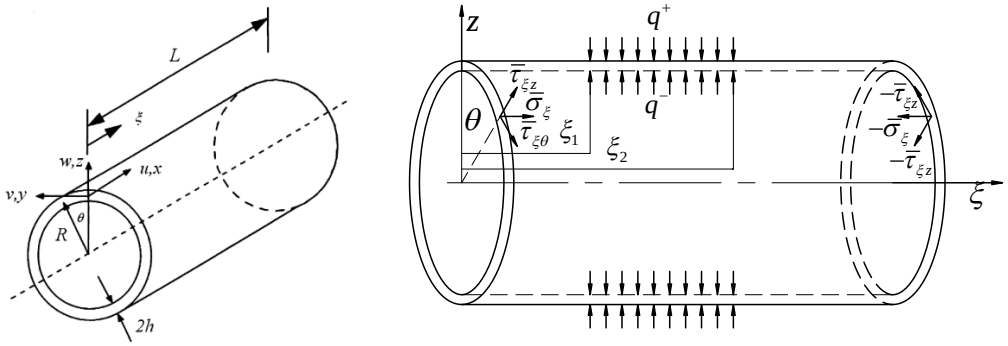

Fig. 1. Geometric parameter of the FGM cylindrical shell, the coordinate system and the schematic calculation of cylindrical shell under the influence of radial concentrated load with boundary conditions at $\xi = 0$, and $\xi = L / R$.

The material parameter variation along the thickness direction is determined as [10]:

$$P_i(z) = P_c + (P_m - P_c)V_m \tag{1}$$

where P_i is the mechanical and physical properties of materials such as Young's

modulus (E), density (ρ), Poisson's ratio (μ); index *m*, *c* denote metal and ceramic, respectively. Voigt's power-volume ratio distribution in the thickness direction is used with $V_m = \left(1/2 + z/2h\right)^{\eta}$, $V_c = 1 - V_m$, in which η is the power factor. It is noteworthy that the ceramic is placed inside the metal.

The displacement of the shell is analyzed as [11]:

$$\begin{aligned} u(\xi,\theta,z) &= u_0(\xi,\theta) + u_1(\xi,\theta)z + u_2(\xi,\theta)z^2/2 + u_3(\xi,\theta)z^3/6, \\ v(\xi,\theta,z) &= v_0(\xi,\theta) + v_1(\xi,\theta)z + v_2(\xi,\theta)z^2/2 + v_3(\xi,\theta)z^3/6, \\ w(\xi,\theta,z) &= w_0(\xi,\theta) + w_1(\xi,\theta)z + w_2(\xi,\theta)z^2/2, \ \xi = x/R. \end{aligned} \tag{2}$$

where u_0, v_0, w_0 are the linear displacements on the neutral surface; u_1, v_1, w_1 denote the midplane rotations of the normal; u_2, v_2, w_2 are the higher-order straight displacements; u_3, v_3 represent the higher-order angular displacement components. Analyzing the displacement field in the form of a sum (Eq. 2) enables us to study the stress-deformation state of a cylindrical shell while taking into account the effect of higher-order shear deformation and transverse-normal stress.

The equilibrium equation system of the shell is determined as [12]:

$$\begin{aligned} &\frac{\partial N_\xi}{\partial \xi} + \frac{\partial N_{\theta\xi}}{\partial \theta} = 0, \ \frac{\partial N_\theta}{\partial \theta} + \frac{\partial N_{\xi\theta}}{\partial \xi} + Q_\theta = 0, \\ &\frac{\partial M_{\xi\theta}}{\partial \xi} + \frac{\partial M_\theta}{\partial \theta} - Q_\theta = 0, \ \frac{\partial M_\xi}{\partial \xi} + \frac{\partial M_{\theta\xi}}{\partial \theta} - RQ_\xi = 0, \\ &\frac{\partial N^*_\xi}{\partial \xi} + \frac{\partial N^*_{\theta\xi}}{\partial \theta} - S_\xi R = 0, \ \frac{\partial N^*_{\xi\theta}}{\partial \xi} + \frac{\partial N^*_\theta}{\partial \theta} - RS_\theta - Q^*_\theta = 0, \\ &\frac{\partial M^*_\xi}{\partial \xi} + \frac{\partial M^*_{\theta\xi}}{\partial \theta} - RQ^*_\xi = 0, \ \frac{\partial M^*_{\xi\theta}}{\partial \xi} + \frac{\partial M^*_\theta}{\partial \theta} - RQ^*_\theta - 2S^*_\theta = 0, \\ &\frac{\partial Q_\xi}{\partial \xi} + \frac{\partial Q_\theta}{\partial \theta} - N_\theta + (R-h)q^- - (R+h)q^+ = 0, \\ &\frac{\partial S_\xi}{\partial \xi} + \frac{\partial S_\theta}{\partial \theta} - M_\theta - RQ_z - \left[(R-h)q^- + (R+h)q^+\right]h = 0, \\ &\frac{\partial Q^*_\xi}{\partial \xi} + \frac{\partial Q^*_\theta}{\partial \theta} - N^*_\theta - RS_z + (R-h)\frac{h^2}{2}q^- - (R+h)\frac{h^2}{2}q^+ = 0. \end{aligned} \tag{3}$$

In the equation system (3), we use the following extrapolation symbols [12]:

$$\left(N_\xi, N_{\xi\theta}, Q_\xi, Q_z\right) = \int_{-h}^{+h} \left(\sigma_\xi, \tau_{\xi\theta}, \tau_{\xi z}, \sigma_z\right)\left(1+\frac{z}{R}\right)dz,$$

$$\left(M_\xi, M_{\xi\theta}, S_\xi, S_z\right) = \int_{-h}^{+h} \left(\sigma_\xi, \tau_{\xi\theta}, \tau_{\xi z}, \sigma_z\right)\left(1+\frac{z}{R}\right)zdz,$$

$$\left(N_\xi^*, N_{\xi\theta}^*, Q_\xi^*\right) = \int_{-h}^{+h} \left(\sigma_\xi, \tau_{\xi\theta}, \tau_{\xi z}\right)\left(1+\frac{z}{R}\right)\frac{z^2}{2}dz, \left(M_\xi^*, M_{\xi\theta}^*\right) = \int_{-h}^{+h} \left(\sigma_\xi, \tau_{\xi\theta}\right)\left(1+\frac{z}{R}\right)\frac{z^3}{6}dz, \quad (4)$$

$$\left(N_{\theta\xi}, N_\theta, Q_\theta\right) = \int_{-h}^{+h} \left(\tau_{\xi\theta}, \sigma_\theta, \tau_{\theta z}\right)dz, \ \left(M_{\theta\xi}, M_\theta, S_\theta\right) = \int_{-h}^{+h} \left(\tau_{\xi\theta}, \sigma_\theta, \tau_{\theta z}\right)zdz,$$

$$\left(N_{\theta\xi}^*, N_\theta^*, Q_\theta^*\right) = \int_{-h}^{+h} \left(\tau_{\xi\theta}, \sigma_\theta, \tau_{\theta z}\right)\frac{z^2}{2}dz, \ \left(M_{\theta\xi}^*, M_\theta^*, S_\theta^*\right) = \int_{-h}^{+h} \left(\tau_{\xi\theta}, \sigma_\theta, \tau_{\theta z}\right)\frac{z^3}{6}dz.$$

where σ_ξ, σ_θ, σ_z are the legal stresses in the respective axes, and $\tau_{\xi\theta}$, $\tau_{\xi z}$, and $\tau_{\theta z}$ are successive stresses.

$$\sum_{n=0}^{3}\left(K_{1n}^m u_n + K_{1n,11}^m \frac{\partial^2 u_n}{\partial\xi^2} + K_{1n,22}^m \frac{\partial^2 u_n}{\partial\theta^2}\right) + \sum_{n=0}^{3} K_{2n,12}^m \frac{\partial^2 v_n}{\partial\xi\partial\theta} + \sum_{n=0}^{2} K_{3n,1}^m \frac{\partial w_n}{\partial\xi} = 0,$$

$$\sum_{n=0}^{3} K_{1n,12}^i \frac{\partial^2 u_n}{\partial\xi\partial\theta} + \sum_{n=0}^{3}\left(K_{2n}^i v_n + K_{2n,11}^i \frac{\partial^2 v_n}{\partial\xi^2} + K_{2n,22}^i \frac{\partial^2 v_n}{\partial\theta^2}\right) + \sum_{n=0}^{2} K_{3n,2}^i \frac{\partial w_n}{\partial\theta} = 0, \quad (5)$$

$$\sum_{n=0}^{3} K_{1n,1}^j \frac{\partial}{\partial\xi} u_n + \sum_{n=0}^{2}\left(K_{3n}^j + K_{3n,11}^j \frac{\partial^2}{\partial\xi^2} + K_{3n,22}^j \frac{\partial^2}{\partial\theta^2}\right) w_n + \sum_{n=0}^{3} K_{2n,2}^j \frac{\partial}{\partial\theta} v_n = K_{43}^j q^+ + K_{53}^j q^-,$$

$$m = 1, 2, 3, 4; \ \ i = 5, 6, 7, 8; \ \ j = 9, 10, 11.$$

where coefficients K depend on the material and geometry parameters of the FGM cylindrical shell. Due to the cumbersome nature of the expressions defining coefficients K, this paper does not present the derivation of these expressions.

The system of partial differential equations (5) is solved using the Laplace transform for single trigonometric series. The details of this process are provided in [11]. The displacement components and the load are expressed as the following single trigonometric series (6):

$$
\begin{aligned}
v_i(\xi,\theta) &= V_{i0}(\xi) + \sum_{m=1}^{\infty} V_{im}(\xi)\sin m\theta, \\
u_i(\xi,\theta) &= U_{i0}(\xi) + \sum_{m=1}^{\infty} U_{im}(\xi)\cos m\theta, \\
w_j(\xi,\theta) &= W_{j0}(\xi) + \sum_{m=1}^{\infty} W_{jm}(\xi)\cos m\theta, \\
q^{\pm}(\xi,\theta) &= \begin{cases} 0, & \text{when } 0 \le \xi < \xi_1,\ \xi_2 < \xi \le L/R, \\ Q_0^{\pm}(\xi) + \sum_{m=1}^{\infty} Q_m^{\pm}(\xi)\cos m\theta, & \text{when } \xi_1 \le \xi \le \xi_2. \end{cases}
\end{aligned} \tag{6}
$$

where $Q_m^{\pm}(\xi)$ are the coefficients of the expansion of the load $q^{\pm}(\xi,\theta)$ in single trigonometric series.

Boundary conditions are required to solve the system of equations (5). In this paper, we only analyze the stress state and the deformation of the FGM cylindrical shell with a double-clamped boundary condition. This is one of the most common types of boundary conditions, and stress concentration can be observed in this case. The double-clamped boundary condition is shown in the following form:

at $\xi = 0, L/R$: $u_i = 0, v_i = 0, w_j = 0,\ (i = 0,1,2,3,\ j = 0,1,2)$.

at $\theta = \theta_1, \theta_2$: $u_i = 0, v_i = 0, w_j = 0\ (i = 0,1,2,3,\ j = 0,1,2)$.

3. Results and discussion

3.1. Validation of the model

For verification calculations, we choose the input parameters according to the literature [13]. The inner surface of the shell is made of Zirconia (ZrO_2), a metal with the following parameters: $\mu_c = 0.2980$, $E_c = 168.06$ (GPa). The outer surface is made of Stainless steel (SUS304) with $\mu_m = 0.3178$, $E_m = 207.79$ (GPa). The shell has a length $L = 0.381$ (m), radius $R = 0.1905$ (m), thickness $2h = 0.000501$ (m). The shell is subjected to uniformly distributed pressure $q_0 = 1000$ (Pa).

Table 1 presents the calculation results of the displacement at $\xi = L/2R$. Analyzing the results, it is shown that the value of the displacement in the middle position according to the quasi-3D theory and that by the semi-analytical finite element model [13] are in good agreement, which can guarantee the validity of the present method.

Tab. 1. The displacement $w\ (m)$ of the FGM cylindrical shell at the middle position

η	60 Elements [13]	90 Elements [13]	120 Elements [13]	Quasi-3D
10	-3,864·10^{-7}	-3,859·10^{-7}	-3,857·10^{-7}	-3,856·10^{-7}
5	-3,794·10^{-7}	-3,789·10^{-7}	-3,787·10^{-7}	-3,786·10^{-7}
1	-3,511·10^{-7}	-3,506·10^{-7}	-3,504·10^{-7}	-3,504·10^{-7}
1/4	-3,289·10^{-7}	-3,284·10^{-7}	-3,282·10^{-7}	-3,282·10^{-7}
1/6	-3,249·10^{-7}	-3,244·10^{-7}	-3,243·10^{-7}	-3,243·10^{-7}
1/8	-3,228·10^{-7}	-3,223·10^{-7}	-3,221·10^{-7}	-3,221·10^{-7}

Figures 2-7 show the displacements and stresses of the shell in a case of external concentrated radial load located at the middle of the shell.

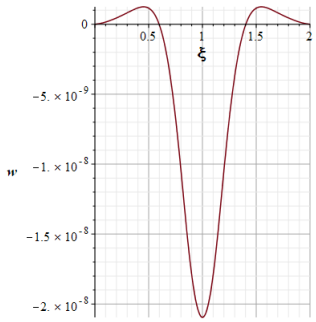

Fig. 2. The displacement w along the shell length

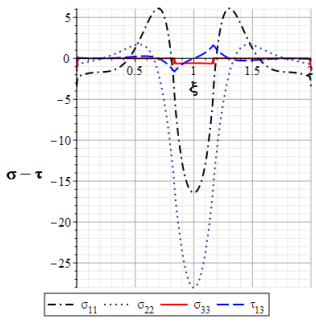

Fig. 3. Distributions of stresses along the shell length

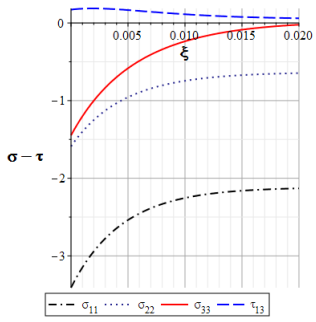

Fig. 4. Distributions of stresses along the shell length at the clamped boundary zone

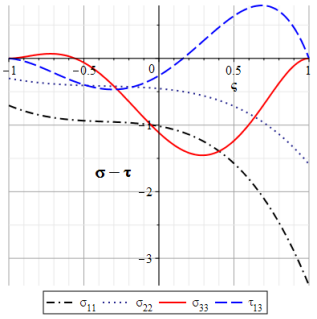

Fig. 5. Distributions of stresses along the shell thickness near the clamped boundary $\xi = 0$

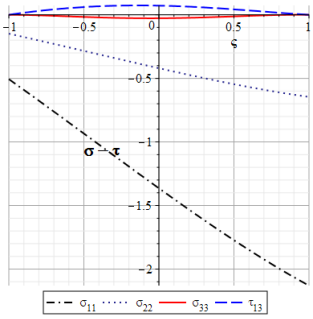

Fig. 6. Distribution of stresses along the shell thickness at a distance $\xi = h / R$

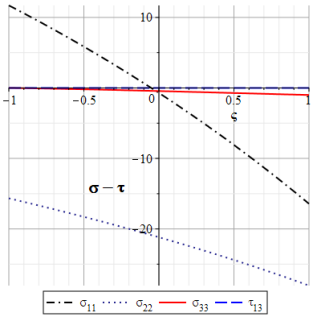

Fig. 7. Stress state along the shell thickness at $\xi = L / 2R$

In particular, the load concentration is defined as follows:

$$q^{+}(\xi,\theta) = \begin{cases} 0, & \text{when } 0 \le \xi < 0.5,\ 1.5 < \xi \le L/R = 2, \\ q_0, & \text{when } 0.5 \le \xi \le 1.5. \end{cases}$$

The stress values shown in the above figures are dimensionless and determined by the following expression:

$$\{\sigma_{11},\ \sigma_{22},\ \sigma_{33},\ \tau_{13}\} = \frac{\{\sigma_{\xi},\ \sigma_{\theta},\ \sigma_{z},\ \tau_{\xi z}\}}{q_0}$$

The results show that stress concentration can be observed near the clamped boundary zone, and it diminishes rapidly as the distance to the boundary increases. In particular, the value of the horizontal stresses σ_{33}, which is ignored in the classical and the first-order theories, is relatively large compared to other stresses.

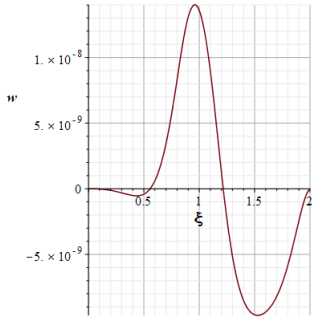

Fig. 8. The displacement w long the shell length

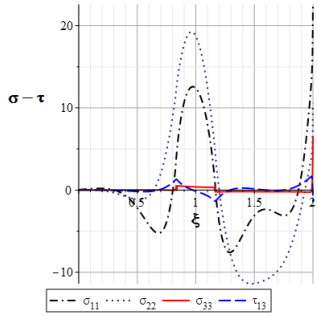

Fig. 9. Distributions of stresses along the shell length

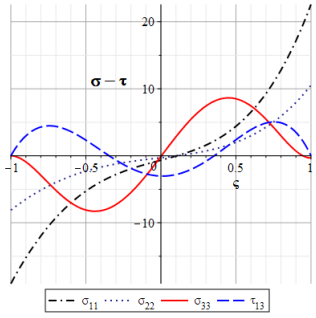

Fig. 10. Distributions of stresses along the shell thickness at the clamped boundary zone $\xi = 2$

Figures 8-10 exhibit the displacement and stresses when the shell is simultaneously subjected to radial, linear and concentrated loads.

$$q^{+}(\xi,\theta) = \begin{cases} 0, & \text{when } 0 \le \xi < 0.5,\ 1.5 < \xi \le L/R = 2, \\ q_0\xi, & \text{when } 0.5 \le \xi \le 1.5. \end{cases}$$

Here, the stress concentration phenomenon at the clamped boundary also appears, which is similar to the prior case.

3.2. Investigate the effect of the shell thickness

To analyze and assess the effect of the thickness on the stress-deformation state, we use the input parameters as stated in Section 3.1. Here, we vary only the relative thickness value. The analysis is only performed for the case of uniformly distributed concentrated load. The displacement and stresses corresponding to various thickness values are presented in Tab. 2.

Tab. 2. Displacement and stresses of the shell while varying the thickness

$\frac{2h}{R}$	$\xi = 0$				$\xi = L/2R$				
	σ_{11}	σ_{22}	σ_{33}	τ_{13}	σ_{11}	σ_{22}	σ_{33}	τ_{13}	$w \times 10^8$
1/10	-2.2584	-1.0520	-0.8681	0.5532	-7.0248	-9.0101	-1.000	0	-0.6159
1/25	-3.4094	-1.5881	-1.4537	0.7948	-16.434	-28.034	-1.000	0	-2.0957
1/50	-6.3622	-2.9635	-2.6748	1.4869	-24.968	-61.654	-1.000	0	-4.9344
1/100	-12.674	-5.9033	-5.3533	2.9020	-26.445	-124.09	-1.000	0	-10.620

Based on the results, it is seen that the shell thickness greatly affects the displacement and stresses. For a shell with a smaller relative thickness value (a thinner shell), greater values of displacement and stresses are obtained. In the boundary region, for thin shells, the displacement and stresses increase with an almost linear law, which is not observed in shells with large relative thickness.

3.3. Investigate the effect of shell length

Similar to Section 3.2, to study the effect of the length on the stress-deformation state of the shell, we vary only the relative length. The displacement and stresses of shells with various relative length values under the effect of distributed concentrated load are presented in Tab. 3.

Analyzing the results, we found that the displacement grows with an increase of the shell length, but not significantly. At $\xi = 0$, the stresses decrease gradually as shell length becomes larger. At $\xi = L/2R$, the normal stress σ_{33} is the same as the applied pressure, and the shear stress $\tau_{13} = 0$ while the remaining stresses decline slightly. When the relative length $L/R \geq 4$, the displacement and the stresses are almost constant.

Tab. 3. Displacement and stresses while varying the length

$\frac{L}{R}$	$\xi = 0$				$\xi = L/2R$				
	σ_{11}	σ_{22}	σ_{33}	τ_{13}	σ_{11}	σ_{22}	σ_{33}	τ_{13}	$w \times 10^8$
1	-4.4219	-1.8771	-2.4326	1.4224	-18.025	-27.877	-1.000	0	-2.0338
2	-3.4094	-1.5881	-1.4537	0.7948	-16.434	-28.034	-1.000	0	-2.0957
4	-1.6436	-0.7656	-0.7017	0.3916	-15.676	-28.024	-1.000	0	-2.1173
6	-1.0928	-0.5090	-0.4666	0.2604	-15.426	-28.021	-1.000	0	-2.1245
8	-0.8185	-0.3813	-0.3495	0.1950	-15.302	-28.020	-1.000	0	-2.1280

3.4. Investigate the effect of material coefficients

The displacement and stresses of shells under the effect of distributed concentrated load corresponding to various values of the material distribution η are given in Tab. 4.

Tab. 4. Displacement and stresses when varying the material distribution coefficient

η	$\xi = 0$				$\xi = L/2R$				
	σ_{11}	σ_{22}	σ_{33}	τ_{13}	σ_{11}	σ_{22}	σ_{33}	τ_{13}	$w \times 10^8$
0.02	-3.2560	-1.5166	-1.4695	0.7998	-15.138	-25.441	-1.000	0	-1.8998
0.05	-3.2627	-1.5197	-1.4706	0.8001	-15.199	-25.577	-1.000	0	-1.9105
0.1	-3.2736	-1.5248	-1.4718	0.8006	-15.297	-25.791	-1.000	0	-1.9273
0.2	-3.2942	-1.5344	-1.4727	0.8010	-15.476	-26.175	-1.000	0	-1.9572
1	-3.4094	-1.5881	-1.4537	0.7948	-16.434	-28.034	-1.000	0	-2.0957
5	-3.5897	-1.6721	-1.3561	0.7241	-18.167	-30.486	-1.000	0	-2.2498
10	-3.6478	-1.6991	-1.3073	0.7247	-18.897	-31.298	-1.000	0	-2.2917
20	-3.3694	-1.7206	-1.2705	0.7011	-19.448	-31.866	-1.000	0	-2.3187
50	-3.7438	-1.7438	-1.2437	0.6839	-19.881	-32.295	-1.000	0	-2.3379

From Tab. 4, it is observed that when increasing the material distribution coefficient, the displacement becomes larger. At $\xi = 0$, the stresses σ_{33} and τ_{13} decrease whereas σ_{11} and σ_{22} increase. At $\xi = L/2R$, σ_{33} is the same as the applied pressure while the shear stress $\tau_{13} = 0$, and the remaining stresses increase. For very large or very small values of η, the stresses and displacement do not show noticeable changes, suggesting that the material distribution coefficient in these cases does not significantly affect the stress-deformation state of the FGM cylindrical shell.

4. Conclusion

Based on the proposed theory and numerical simulations in this work, we have some principal conclusions as follows:

- The paper presented the theoretical basis and numerical analysis in calculating the FGM cylindrical shell under local load based on the quasi-3D higher-order shear deformation theory. The validity of the research method and the calculation program has been confirmed in a comparison with the results from a previous paper.

- Analyses of the effects of several shell geometric parameters (thickness and length) and the material distribution coefficient on the stress-deformation state of the shell were carried out for the case of uniformly concentrated distribution of radial load.

- An analysis of stress concentration phenomenon in the clamped boundary zone was conducted. In this zone, the value of the horizontal-normal stresses σ_{33}, which is ignored in the classical and the first-order theories, is relatively large compared to other stresses. Therefore, to accurately assess structural strength in the boundary area, it is necessary to use a quasi-3D higher-order shear deformation theory.

References

1. Birman, V., & Byrd, L. W. (2007). Modeling and Analysis of Functionally Graded Materials and Structures. *Applied Mechanics Reviews, 5*(60), 195-216.
2. Bishay, P. L., Sladek, J., Sladek, V., & Atluri, S. N. (2012). Analysis of functionally graded magneto-electro-elastic composites using hybrid/mixed finite elements and node-wise material properties. *Computers, Materials & Continua, 29*(3), 213.
3. Miyamoto, Y., Kaysser, W. A., Rabin, B. H., Kawasaki, A., & Ford, R. G. (Eds.) (2013). *Functionally graded materials: Design, processing and applications*, Springer Science & Business Media.
4. Kirchhoff, G. (1850). Uber das gleichgewicht und die bewegung einer elastischen scheibe. *Journal Fur Die Reine und Angewandte Mathematik, 1850*(40), 51-88.
5. Mindlin, R. (1951). Influence of rotatory inertia and shear on flexural motions of isotropic, elastic plates. *Journal of Applied Mechanics, 1*(18), 31-38.
6. Reddy, J. N. (1984). A simple higher-order theory for laminated composite plates. *Journal of applied mechanics, 51*(4), 745-752.
7. Duc, N. D. (2016). Nonlinear thermal dynamic analysis of eccentrically stiffened S-FGM circular cylindrical shells surrounded on elastic foundations using the Reddy's third-order shear deformation shell theory. *European Journal of Mechanics-A/Solids, 58*, 10-30.
8. Duc, N. D. (2018). Nonlinear thermo- electro-mechanical dynamic response of shear deformable piezoelectric sigmoid functionally graded sandwich circular cylindrical shells on elastic foundations. *Journal of Sandwich Structures & Materials, 20*(3), 351-378.
9. Voigt, W. (1889). Ueber die Beziehung zwischen den beiden Elasticitätsconstanten isotroper Körper. *Ann. Phys., 74*(12), 573-87.
10. Hui-Shen Shen (2009). *Functionally Graded Materials: Nonlinear Analysis of Plates and Shells*, CRC Press.
11. Firsanov, V. V., and Doan, T. N. (2015). Investigation of the statics and free vibrations of cylindrical shells on the basis of a nonclassical theory. *Composites: Mechanics, Computations, Applications: An International Journal, 6*(2), 135-166.
12. Trần Ngọc Đoàn, Vũ Quốc Trụ, Trần Văn Hùng (2019). Khảo sát trạng thái ứng suất-biến dạng của vỏ trụ FGM trên cơ sở lý thuyết biến dạng trượt bậc cao kiểu Quasi-3D. *Tạp chí Khoa học và Kỹ thuật, 201*(8-2019), Học viện KTQS, 24-33.
13. Santos, H., Soares, C. M. M., Soares, C. A. M., & Reddy, J. N. (2009). A semi-analytical finite element model for the analysis of cylindrical shells made of functionally graded materials. *Composite Structures, 91*(4), 427-432.

PHÂN TÍCH TĨNH VỎ TRỤ FGM CHỊU TẢI TRỌNG TẬP TRUNG SỬ DỤNG LÝ THUYẾT BIẾN DẠNG TRƯỢT BẬC CAO KIỂU QUASI-3D

Tóm tắt: *Bài báo trình bày kết quả phân tích tĩnh vỏ trụ có cơ tính biến thiên (FGM) chịu tải trọng tập trung theo hướng tiếp cận giải tích. Các phương trình cơ bản được xây dựng dựa trên lý thuyết biến dạng trượt bậc cao, có tính đến ảnh hưởng của ứng suất và biến dạng cắt ngang. Đặc tính phân bố vật liệu một chiều theo chiều dày với quy luật phân bố lũy thừa Voigt. Trong bài báo, các tác giả nghiên cứu ảnh hưởng của một số tham số hình học (chiều dày, chiều dài vỏ), hệ số phân bố vật liệu lên trạng thái ứng suất của vỏ trụ FGM. Thông qua phân tích trạng thái ứng suất vỏ tại vị trí biên ngàm, chứng minh hiện tượng tập trung ứng suất tại vùng biên, đồng thời khẳng định giá trị ứng suất pháp ngang là không thể bỏ qua trong tính toán kết cấu tại vùng biên này.*

Từ khóa: Vỏ trụ; FGM; lý thuyết biến dạng pháp và trượt bậc cao; trạng thái ứng suất biến dạng; hiện tượng tập trung ứng suất.

Received: 07/02/2020; *Revised:* 21/7/2020; *Accepted for publication:* 28/7/2020

❑